Static and dynamic magnetic properties of circular and square cobalt nanodots in hexagonal cells

Franco N. Mélica[a], Eduardo Saavedra[b], Juan Escrig[b,c], Noelia Bajales[d,e], Omar E. Linarez Pérez[a,f]*, Diana M. Arciniegas Jaimes[a,f]**

[a]*Universidad Nacional de Córdoba, Facultad de Ciencias Químicas, Departamento de Fisicoquímica, Haya de la Torre esq. Medina Allende, X5000HUA Córdoba, Argentina.*
[b]*Departamento de Física, Universidad de Santiago de Chile (USACH), Av. Víctor Jara 3493, 9170124 Santiago, Chile.*
[c]*Center for the Development of Nanoscience and Nanotechnology (CEDENNA), 9170124 Santiago, Chile.*
[d]*Universidad Nacional de Córdoba, FAMAF, 5000 Córdoba, Argentina.*
[e]*CONICET, IFEG, Av. Medina Allende s/n, 5000 Córdoba, Argentina.*
[f]*CONICET, INFIQC, Haya de la Torre esq. Medina Allende, X5000HUA, Córdoba, Argentina.*

*olinarez@unc.edu.ar
**diana.arciniegas@unc.edu.ar

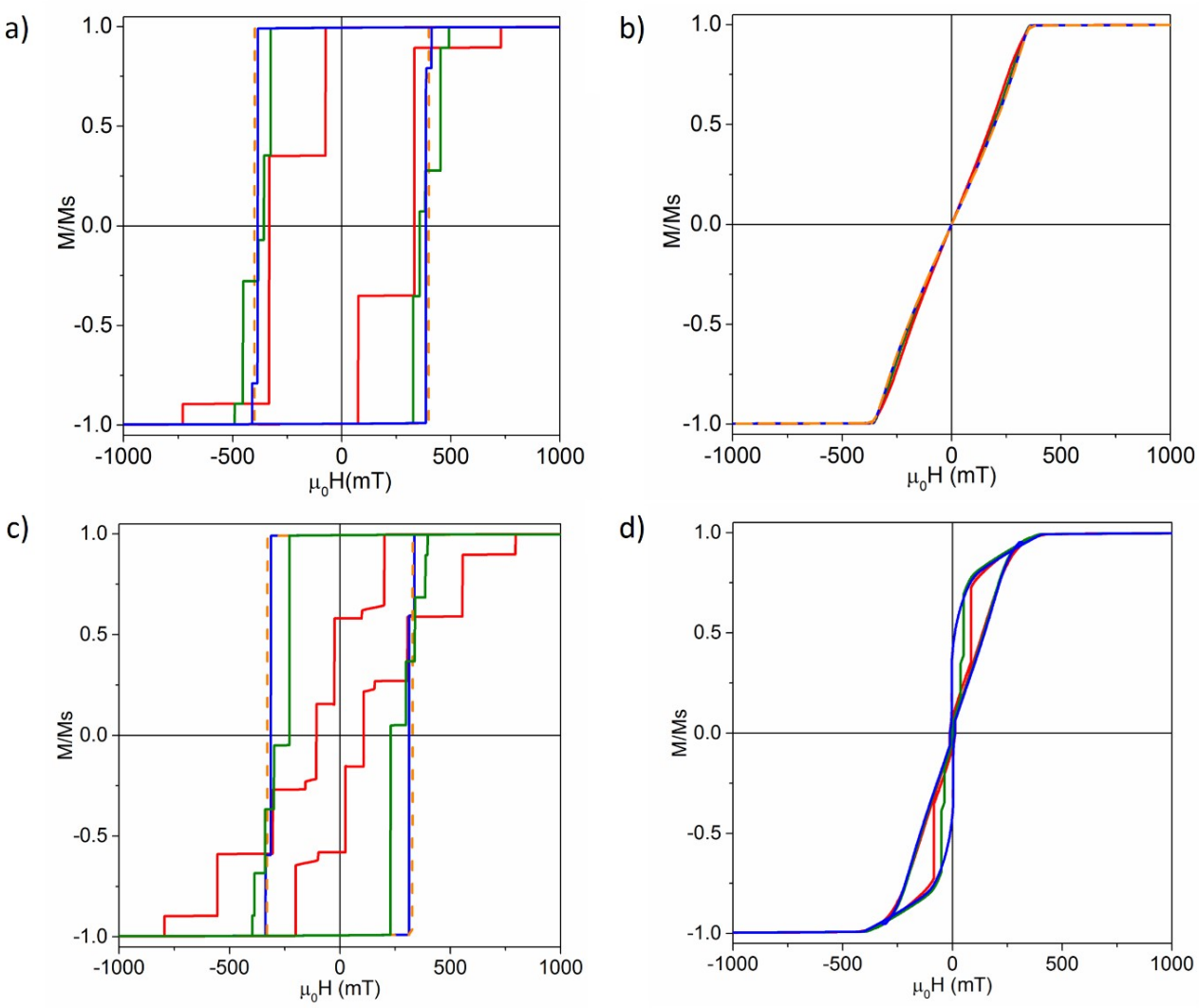

Figure S1. Hysteresis curves for a hexagonal cell of nineteen circular nanodots (second-nearest neighbors) when the external magnetic field is applied along **(a)** *z*-axis and **(b)** *x*-axis. Hysteresis curves for a hexagonal cell of nineteen square nanodots (second-nearest neighbors) when the external magnetic field is applied along **(c)** *z*-axis and **(d)** *x*-axis. For all the curves: d_{cc}=1.25d (—), 1.75d (—), 2.5d (—) and 3d (- - - -).

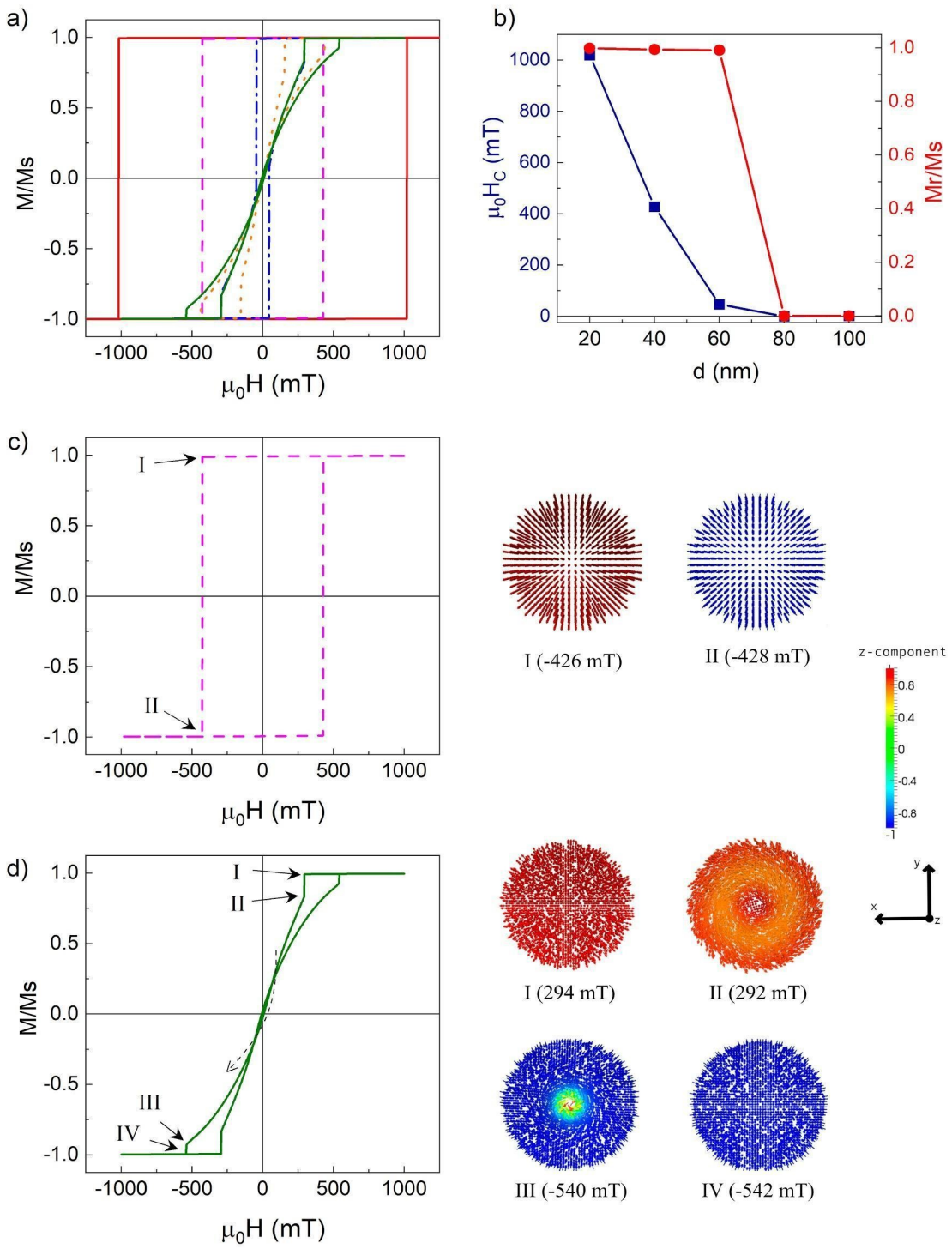

Figure S2. (a) Hysteresis curves of an isolated circular nanodot when the external magnetic field is applied along the *z*-axis. Circular nanodots with diameters of 20 nm (—), 40 nm (– – – –), 60 nm (· – · –), 80 nm (· · · ·) and 100 nm (—) are considered. **(b)** Coercivity (■) and reduced remanence (●) as a function of nanodot diameter. **(c)** Hysteresis curve for a 40 nm diameter circular nanodot and snapshots of the magnetization at the point on the hysteresis curve that are highlighted. **(d)** Hysteresis curve for a 100 nm diameter circular nanodot and snapshots of the magnetization at the point on the hysteresis curve that are highlighted.

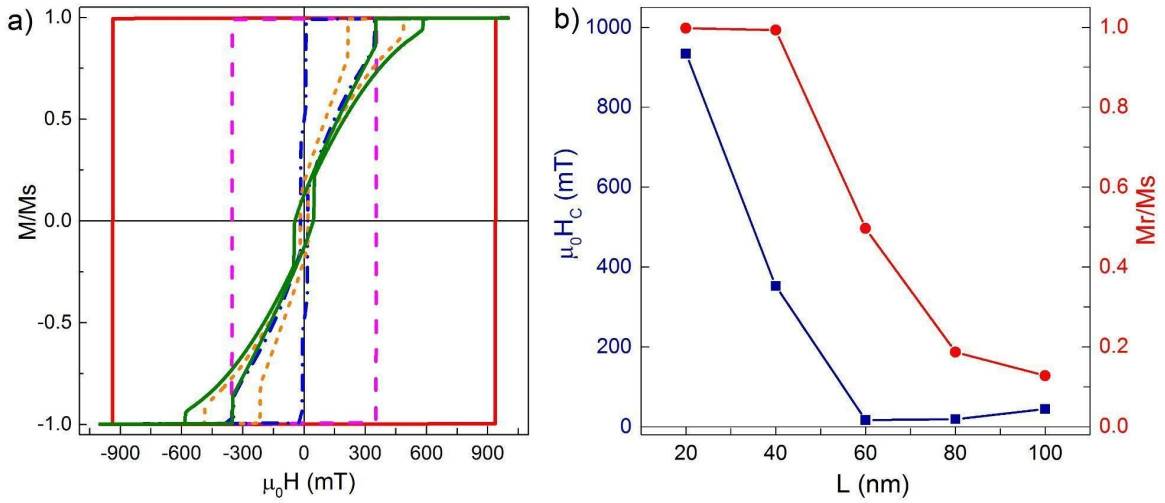

Figure S3. (a) Hysteresis curves of an isolated square nanodot when the external magnetic field is applied along the *z*-axis. Square nanodots with lengths of 20 nm (—), 40 nm (– – – –), 60 nm (· – · –), 80 nm (· · · ·) and 100 nm (—) are considered. (b) Coercivity (■) and reduced remanence (●) as a function of nanodot length.

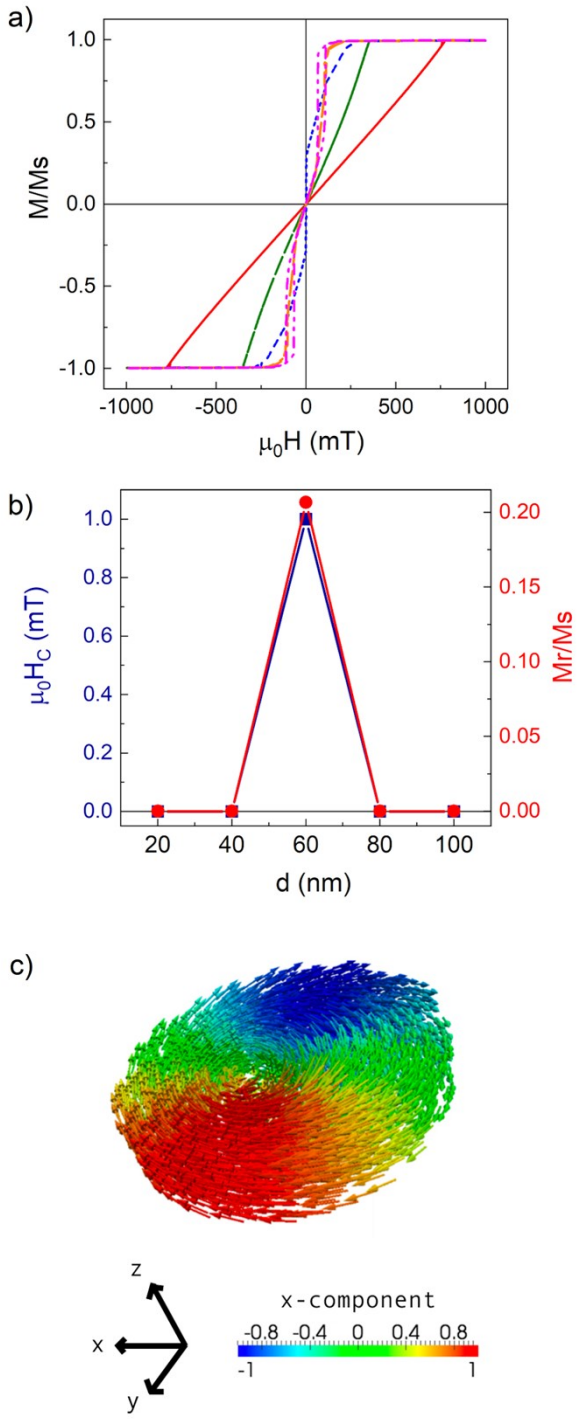

Figure S4. (a) Hysteresis curves of an isolated circular nanodot when the external magnetic field is applied along the *x*-axis. Circular nanodots with diameters of 20 nm (—), 40 nm (– – – –), 60 nm (· – · –), 80 nm (· · · ·) and 100 nm (—) are considered. **(b)** Coercivity (■) and reduced remanence (●) as a function of nanodot diameter. **(c)** Vectorial representation of the magnetic vortex configuration with c = -1 and p = +1 obtained for a 100 nm diameter circular nanodot in the absence of an external magnetic field.

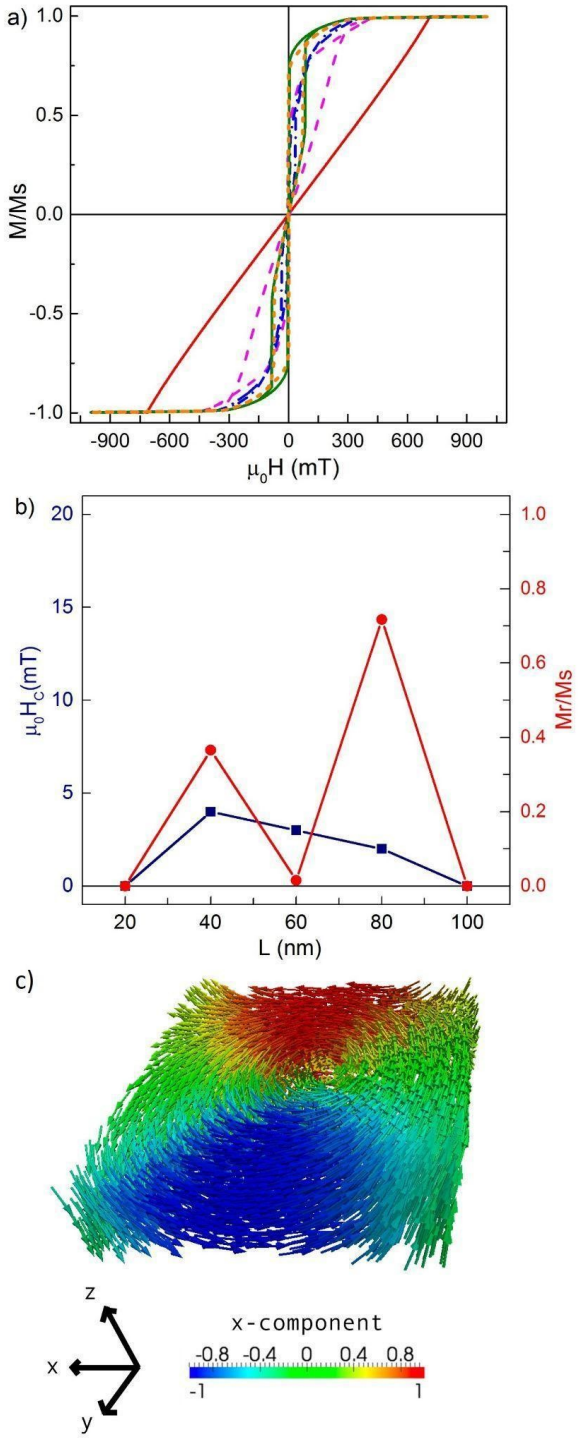

Figure S5. (a) Hysteresis curves of an isolated square nanodot when the external magnetic field is applied along the *x*-axis. Square nanodots with lengths of 20 nm (—), 40 nm (– – – –), 60 nm (· – · –), 80 nm (· · · ·) and 100 nm (—) are considered. **(b)** Coercivity (■) and reduced remanence (●) as a function of nanodot length. **(c)** Vectorial representation of the magnetic vortex configuration with c = -1 and p = +1 obtained for a 100 nm length square nanodot in the absence of an external magnetic field.

Table S1: Resonant frequencies of the circular and square nanodot arrays when a fixed external magnetic field of 1000 mT is applied in the *z*-direction and a sinc-wave excitation field is applied in the *y*-direction.

Center-to-center distance, dcc (nm)	Mode 1 Circle (GHz)	Mode 1a Circle (GHz)	Mode 1 Square (GHz)	Mode 1a Square (GHz)
1.25d	34.7	32	30.25	26.35
1.75d	37.55	36.75	34.95	33.8
2.5d	38.3	--	35.95	--
3.0d	38.6	--	36.35	--

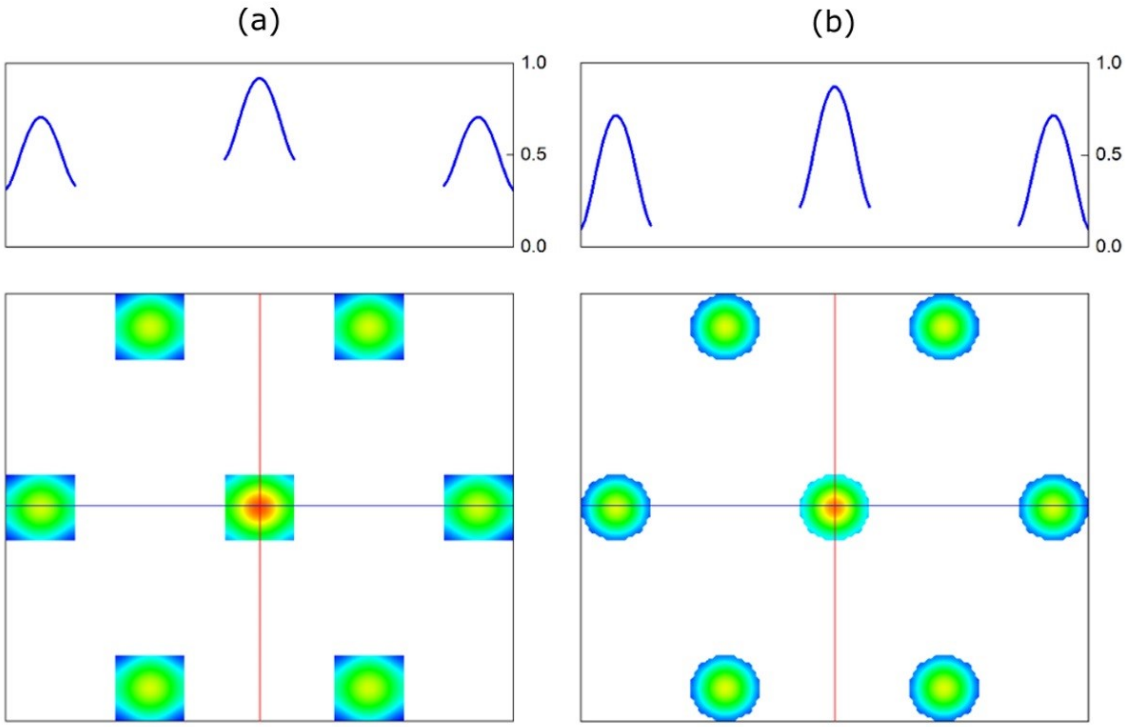

Figure S6. Profile of the 1_s and 1_c resonance modes for the **(a)** square and **(b)** circular nanodot arrays, when we apply a fixed external magnetic field of 1000 mT in the *z*-direction and a sinc wave excitation field in the *y*-direction.

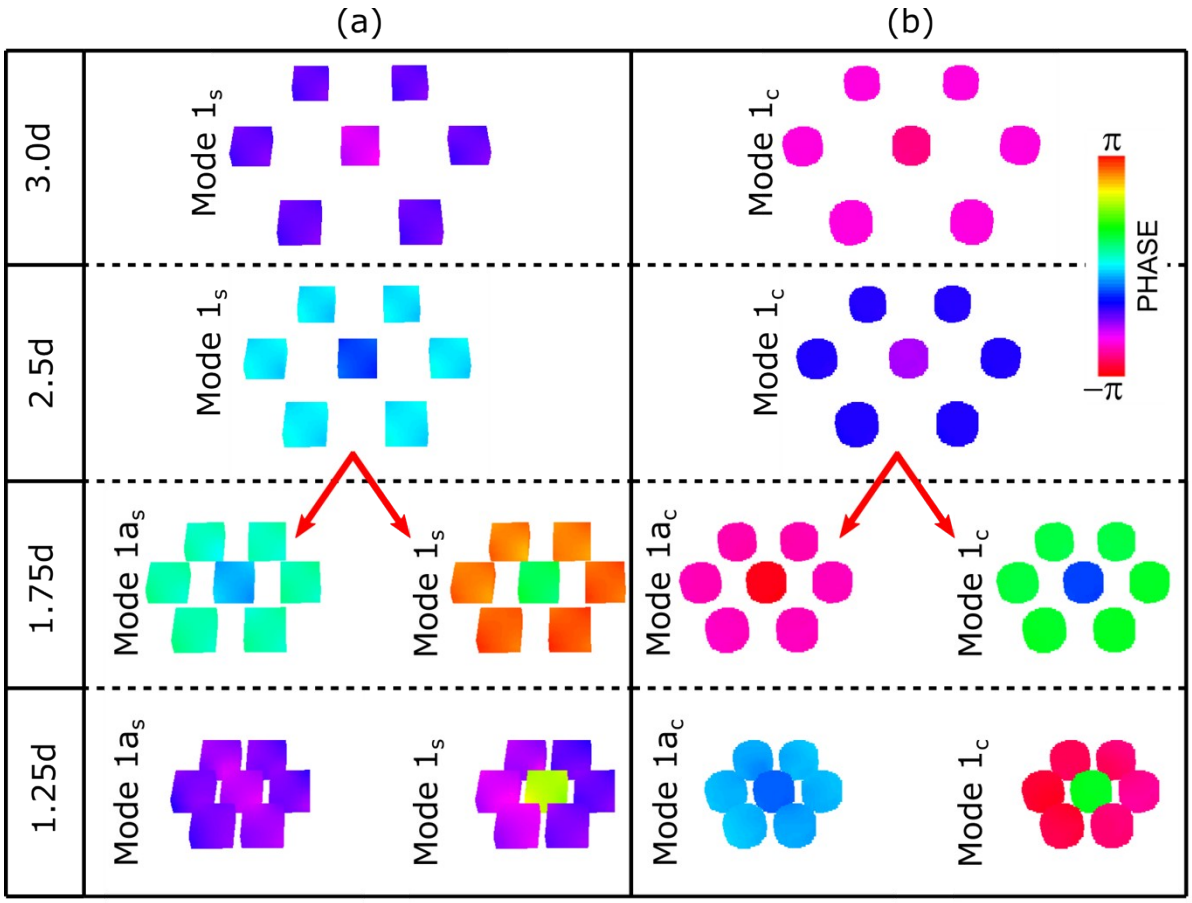

Figure S7. Spatial distribution of the phases corresponding to the spectra of the resonant modes for arrays of **(a)** square and **(b)** circular nanodots obtained when a fixed external magnetic field of 1000 mT is applied in the *z*-direction and a sinc wave excitation field in the *y*-direction. The rows correspond to different values of center-to-center distance between the nanodots. The color code establishes the phase of the FFT used in the *y*-component of the magnetizing field.

Table S2: Resonant frequencies of the circular and square nanodot arrays when a fixed external magnetic field of 1000 mT is applied in the *x*-direction and a sinc-wave excitation field is applied in the *y*-direction.

Center-to-center distance, dcc (nm)	Mode 1 Square (GHz)	Mode 2 Square (GHz)	Mode 1a Square (GHz)	Mode 1b Square (GHz)	Mode 1b_a Square (GHz)	Mode 1b_b Square (GHz)
1.25d	--	46.2	20.9	--	23.65	26.55
1.75d	--	44.5	21.3	23.6	--	--
2.5d	22.45	43.95	--	--	--	--
3.0d	22.25	43.85	--	--	--	--
Center-to-center distance, dcc (nm)	**Mode 1 Circle (GHz)**	**Mode 2 Circle (GHz)**	**Mode 1a Circle (GHz)**	**Mode 1b Circle (GHz)**	**Mode 1b_a Circle (GHz)**	**Mode 1b_b Circle (GHz)**
1.25d	--	--	23.35	--	25.65	27.65
1.75d	--	--	23.1	23.65	--	--
2.5d	22.75	--	--	--	--	--
3.0d	22.55	--	--	--	--	--

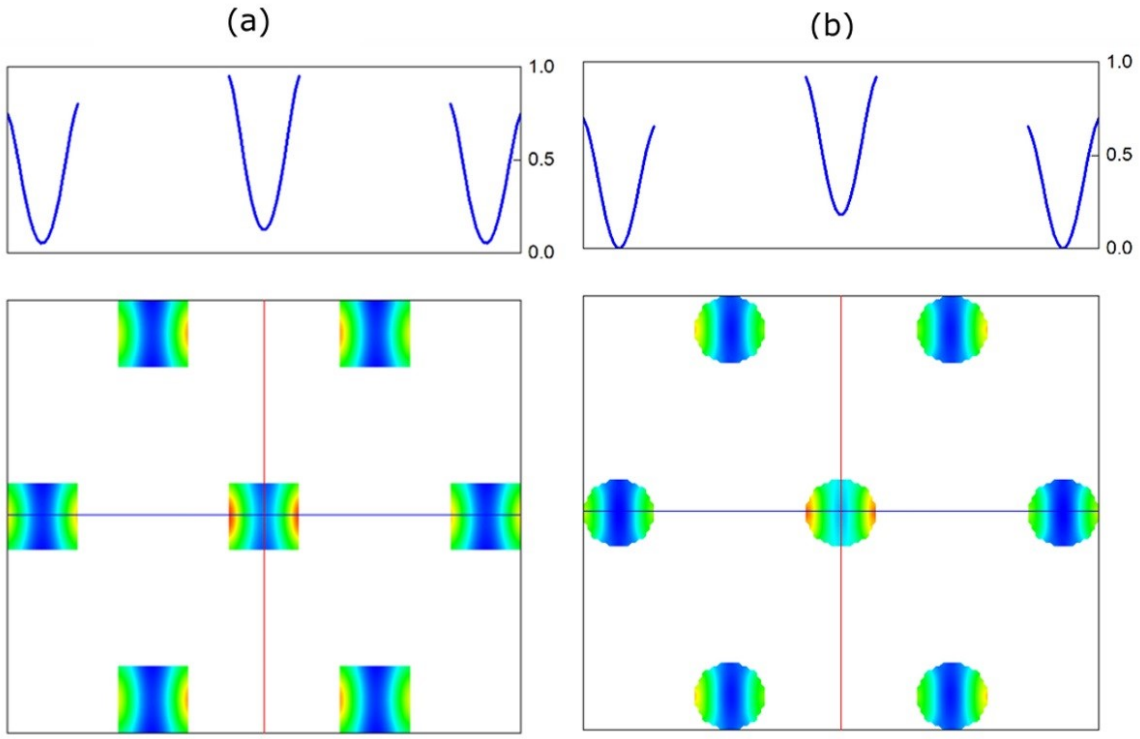

Figure S8. Profile of the 1_s and 1_c resonance modes for the **(a)** square and **(b)** circular nanodot arrays, respectively, when we apply a fixed external magnetic field of 1000 mT in the *x*-direction and a sinc wave excitation field in the *y*-direction.

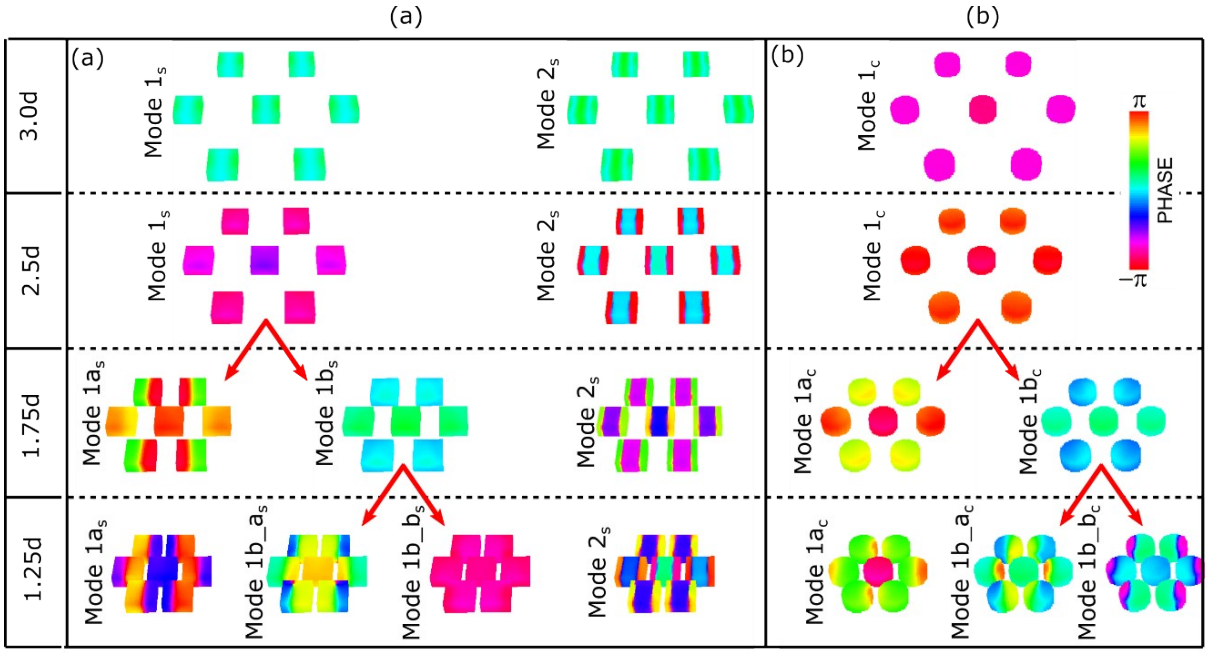

Figure S9. Spatial distribution of the phases corresponding to the spectra of the resonant modes for arrays of **(a)** square and **(b)** circular nanodots obtained when a fixed external magnetic field of 1000 mT is applied in the *x*-direction and a sinc wave excitation field in the *y*-direction. The rows correspond to different values of center-to-center distance between the nanodots. The color code establishes the phase of the FFT used in the *y*-component of the magnetizing field.

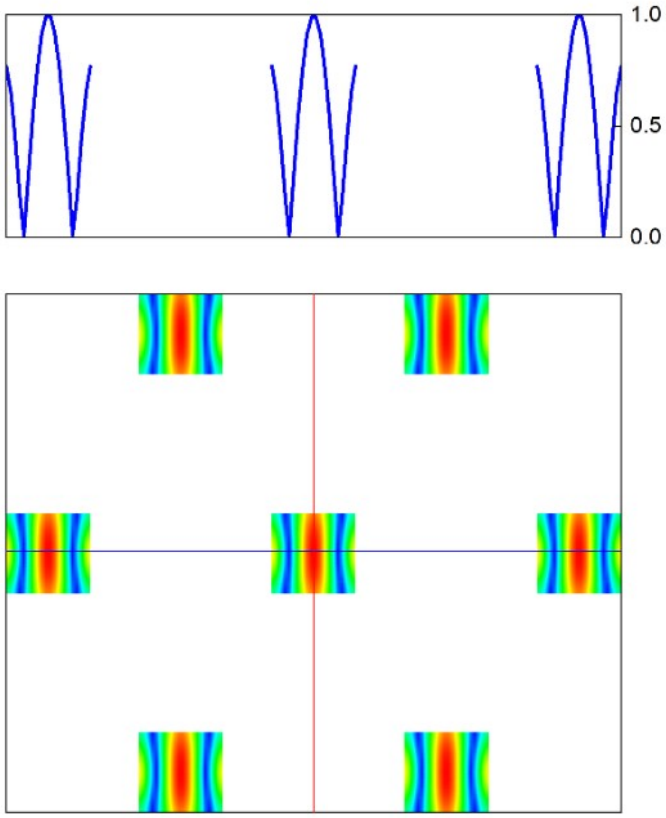

Figure S10. Profile of the 2_s resonance mode for the square nanodot arrays when we apply a fixed external magnetic field of 1000 mT in the *x*-direction and a sinc wave excitation field in the *y*-direction. This profile shows a localized mode with two nodal line.

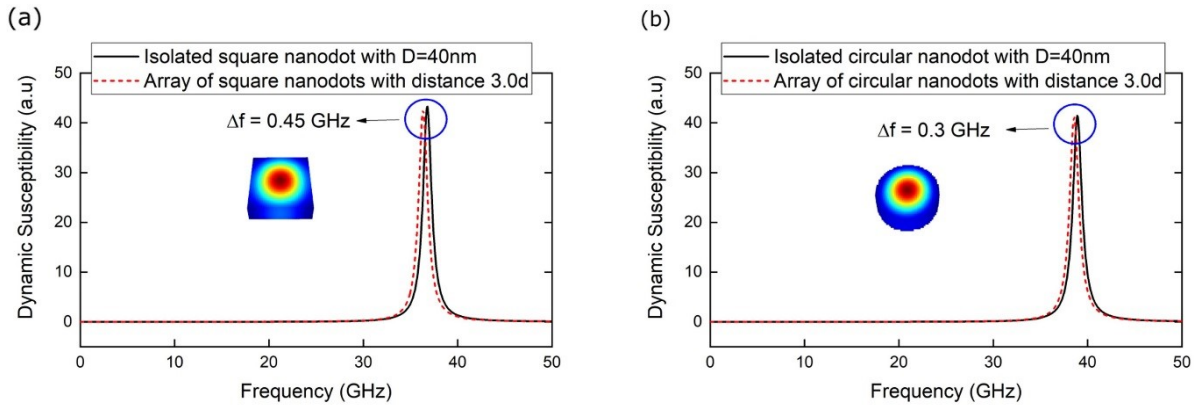

Figure S11. Comparison between the dynamic susceptibility measured for an array of nanodots separated at a distance of 3.0d and an isolated nanodot in the presence of a fixed magnetic field of 1000 mT applied along the *z*-axis for **(a)** square and **(b)** circular nanodots.

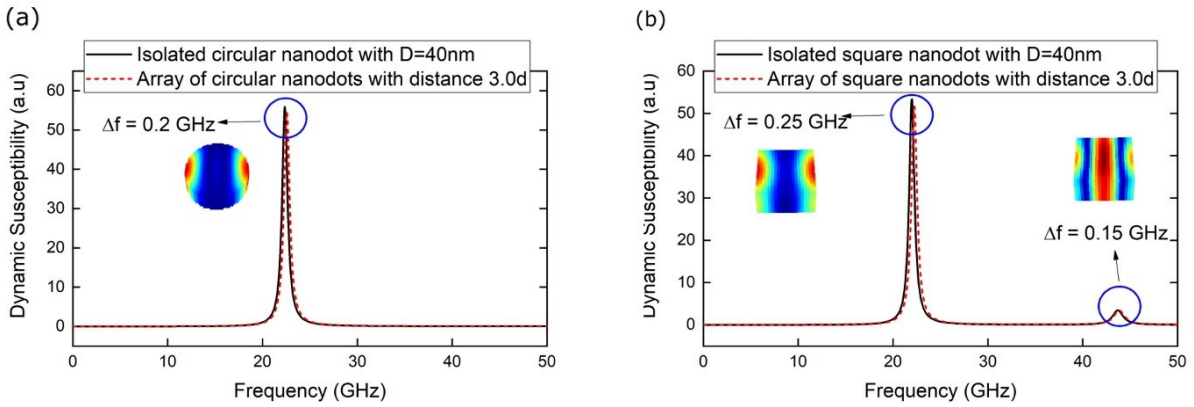

Figure S12. Comparison between the dynamic susceptibility measured for an array of nanodots separated at a distance of 3.0d and an isolated nanodot in the presence of a fixed magnetic field of 1000 mT applied along the *x*-axis for **(a)** square and **(b)** circular nanodots.